

The Detection of Pure Dark Matter Objects with Bent Multiply Imaged Radio Jets

R. Benton Metcalf

Institute of Astronomy, University of Cambridge, Cambridge CB3 0HA, UK

ABSTRACT

When a gravitational lens produces two or more images of a quasar's radio jet the images can be compared to reveal the presents of small structures along one or more of the lines of sight. If mass is distributed smoothly on scales of $\lesssim 10^7 M_\odot$ independent bends in the jet images on milli-arcsecond scales will not be produced. Both of the two multiply imaged radio jets that have been mapped on milli-arcsecond scales show some evidence of this bending. Using existing data we model the lens system B1152+199 and show that it contains a substructure of mass $\sim 10^7 h^{-1} M_\odot$ or a velocity dispersion of $\sim 10 \text{ km s}^{-1}$. We then investigate the probability of a radio jet being bent by small scale structure both inside and outside of the host lens. The known populations of dwarf galaxies and globular clusters are far too small to make this probability acceptable. A previously unknown population of massive dark objects is needed. The standard Cold Dark Matter (CDM) model might be able to account for the observations if small mass halos are sufficiently compact. In other cosmological models where small scale structure is suppressed, such as standard Warm Dark Matter (WDM), the observed bent jets would be very unlikely to occur.

1. Introduction

The standard Λ CDM cosmological model has been very successful in accounting for observations on scales larger than around a Mpc. However, it appears that this model faces difficulties on the scales of galaxies and dwarf galaxies (van den Bosch et al. 2000). One such problem is that CDM simulations of the local group of galaxies predict an order of magnitude more dwarf galaxy halos with masses greater than $\sim 10^7 M_\odot$ than there are observed satellites of the Milky Way (MW) Galaxy and M31 (Moore et al. 1999; Klypin et al. 1999; Mateo 1998). These simulations predict that 10-15% of the virial mass of a galaxy halo is in substructures of mass $\gtrsim 10^7 M_\odot$.

This over prediction of dwarf halos could be a sign that there is something fundamentally wrong with the CDM model. Proposed explanations include warm dark matter (WDM) which smoothes out small scale structure in the early universe (e.g. Bode, Ostriker, & Turok 2001), unorthodox inflation models which break scale invariance (Kamionkowski & Liddle 2000) and self-interacting dark matter which causes substructures to evaporate within larger halos (Spergel & Steinhardt 2000). Alternatively, CDM could be correct and the small Dark Matter (DM) clumps could exist, but not contain stars, so as to escape detection as observable dwarf galaxies. This situation can easily, perhaps inevitably, come about through the action of feedback processes (radiation and supernova winds) from the first generation of stars in the universe e.g. Bullock, Kravtsov, & Weinberg (2000); Somerville (2002). For example, photoionization can prevent gas from cooling and thus inhibit star formation in halos that are too small to be self-shielding. Several authors, (e.g. Metcalf 2001), have argued that the overabundance of DM clumps is likely to extend down to smaller masses and larger fractions of the halo mass than have thus far been accessible to numerical simulations. These nearly pure dark matter structures have largely been considered undetectable.

Mao & Schneider (1998) first proposed substructure as an explanation for the magnification ratios of the 4-image quasar lenses B1422+231 which do not agree with any simple lens model. The modeling of B1422+231 has since been improved in Bradač et al. (2002) and Keeton (2002). It still appears that a substructure with a mass of $10^4 - 10^7 h^{-1} M_{\odot}$ near image A is required to explain the difference between the radio and optical flux ratios in this system. Metcalf & Madau (2001) showed that if CDM substructure exists it could be detected through the magnification ratios of 4-image quasar lenses. Concurrently Chiba (2002) modeled three 4-image lenses and showed that a significant amount of substructure was necessary to make their magnification ratios agree with simple smooth lens models. These ideas have been further investigated in Metcalf & Zhao (2002) and Dalal & Kochanek (2002). These studies all rely on the influence of substructure on magnification ratios. This is a promising approach, but it is strongly model dependent and susceptible to misinterpretation because of microlensing by ordinary stars in the lens galaxy, even at radio wavelengths.

It was also predicted in Metcalf & Madau (2001) that CDM substructure, if it exists, should occasionally distort multiply imaged radio jets on milli-arcsecond scales. This distortion would not be reproduced in all the images so it can be distinguished from structure in the jet itself. This effect had also been suggested by Wambsganss & Paczynski (1992) as a method for detecting a large abundance of $m \gtrsim 10^6 M_{\odot}$ primordial black holes. As will be demonstrated here, this method has the important advantages of avoiding confusion with microlensing and avoiding any strong dependence on the lens model.

In section 2 the observations of mapped multiply imaged radio jets are summarized. In section 3 general considerations related to modeling multiply imaged radio jets are discussed and specific models for a particular case are presented. The interpretation of these results in terms of the level of small scale structure in the universe is addressed in § 4. General discussion and conclusions are in § 5.

In this paper the Hubble parameter is $H_0 = 65 h_{65} \text{ km s}^{-1} \text{ Mpc}^{-1}$.¹ For quantities that do not have a simple dependence on H_o a value $h_{65} = 1$ is used. The present average density of matter in the universe in units of the critical density is Ω_m and the cosmological constant in the same units is Ω_{Λ} . The “concordance” cosmological model ($\Omega_m = 0.3$, $\Omega_{\Lambda} = 0.7$) will be assumed throughout. Milli-arcseconds will be abbreviated as mas.

2. Observations of multiply imaged radio jets

The two image gravitational lens B1152+199 was discovered in the CLASS radio survey and follow-up observations were done on the Keck II telescope (Myers et al. 1999). The images are separated by $1''.56$ and the redshifts of the source and lens are $z_s = 1.019$ and $z_l = 0.439$. Subsequently, Rusin et al. (2002) observed B1152+199 using the Hubble Space Telescope (HST), the Multi-Element Radio-Linked Interferometer Network (MERLIN) and the Very Long Baseline Array (VLBA). In the HST observations a faint, indistinct lens galaxy can be seen. With VLBA they were able to map the two images of the radio jet on milli-arcsecond scales. They discovered that in image A the jet appears straight while in image B it is bent. It is this bend that we seek to explain and interpret in this paper. The bend is clearly not aligned with either the direction to image A or to the lens galaxy. Superluminal motion is a possible explanation only if the jet’s shape can change on a time scale that is smaller than the time delay between images. Rusin et al. (2002) fit a variety of smooth models to the macroscopic lens and get time delays of 26.7 to 45.9 h^{-1} days

¹On a couple of occasions when quoting other peoples work the convention $H_0 = 100 h \text{ km s}^{-1} \text{ Mpc}^{-1}$ is used.

which making this an unlikely explanation. They do not attempt to explain the bend with their lens models.

As far as we are aware, there is only one other multiply imaged radio jet that has been mapped on milli-arcsecond scales, Q0957+561. This was the first gravitational lens discovered (Walsh, Carswell, & Weymann 1979) and has been studied extensively in the past two decades. The VLBI maps of the radio jets appear to show a kink in image A that is not reproduced in image B (near $\Delta\delta = 20$ mas, $\Delta\alpha = 10$ mas with respect to the core) (Garrett et al. 1994; Barkana et al. 1999). Although in this case the bend is much less distinct than in B1152+199 – and we will not try to reproduce it with a lens model here – it does suggest that milli-arcsecond kinks and bends are common. This has very important consequences in relation to the discussion in § 4, because it implies that the bend in B1152+199 is not just a rare coincidental alignment of the image and a substructure.

3. Modeling the Jet

3.1. Formalism

The radio jet will be treated as a one dimensional curve on the sky described by $\vec{\theta}_{\text{source}}(s)$ in the absence of lensing. An image of the jet is described by $\vec{\theta}_{\text{image}}(s)$. The curve of the source jet is related to the curve of its image through the lensing equation

$$\mathbf{y}(s) = \mathbf{x}(s) - \nabla\psi(\mathbf{x}(s)) \quad (1)$$

$$\mathbf{y}(s) \equiv D_l \vec{\theta}_{\text{source}}(s) / \lambda_o \quad \mathbf{x}(s) \equiv D_l \vec{\theta}_{\text{image}}(s) / \lambda_o \quad (2)$$

where λ_o is an arbitrary scaling length and s is the arc-length along the jet in the image plane measured in the same units as \mathbf{x} . The angular size distances to the lens, source, and from the lens to the source will be denoted D_l , D_s , and D_{ls} respectively. The lensing potential is related to the lens surface density, $\Sigma(\mathbf{x})$, through the Poisson equation $\nabla^2\phi(\mathbf{x}) = 2\kappa(\mathbf{x})$ where $\kappa \equiv \Sigma(\mathbf{x})/\Sigma_c$. The critical surface density is defined as $\Sigma_c = (4\pi G D_l D_{ls} / c^2 D_s)^{-1}$.

The tangent and normal vectors of the jet are given by

$$\mathbf{t}(s) \equiv \frac{\partial \mathbf{x}}{\partial s} \quad \mathbf{n}(s) \equiv \frac{\partial^2 \mathbf{x}}{\partial s^2}. \quad (3)$$

The magnitudes of these vectors are $t(s) = 1$ and $n(s) = 1/R(s)$ where $R(s)$ is the radius of curvature. For convenience we define the matrices

$$\mathbf{A}_{ij} \equiv \delta_{ij} - \frac{\partial^2 \psi}{\partial x^i \partial x^j} \quad \mathbf{M}_{ijk} \equiv -\frac{\partial^3 \psi}{\partial x^i \partial x^j \partial x^k}. \quad (4)$$

Now we can find the curvature and normal vectors to the source jet by taking derivatives of the lens equation

$$\mathbf{T}(s) \equiv \frac{\partial \mathbf{y}}{\partial s'} = \frac{\partial s}{\partial s'} \frac{\partial \mathbf{y}}{\partial s} = \frac{\mathbf{u}}{|\mathbf{u}|} \quad (5)$$

$$\mathbf{N}(s) \equiv \frac{\partial^2 \mathbf{y}}{\partial s'^2} = \left(\frac{\partial s}{\partial s'} \right)^2 \frac{\partial^2 \mathbf{y}}{\partial s^2} + \frac{\partial^2 s}{\partial s'^2} \frac{\partial \mathbf{y}}{\partial s} = \frac{1}{|\mathbf{u}|^2} \left(\mathbf{v} - \frac{\mathbf{u}(\mathbf{v} \cdot \mathbf{u})}{|\mathbf{u}|} \right), \quad (6)$$

$$\mathbf{u}_i \equiv \sum_j \mathbf{A}_{ij} \mathbf{t}_j \quad \mathbf{v}_i \equiv \sum_j \mathbf{A}_{ij} \mathbf{n}_j + \sum_{jk} \mathbf{M}_{ijk} \mathbf{t}_j \mathbf{t}_k \quad (7)$$

where s' is the arc-length on the source plane. The vectors $\mathbf{T}(s)$ and $\mathbf{N}(s)$ must be the same for all images of the jet so they can be used as constraints on the lens model. Along with the position coordinates on the source plane this makes 4 constraints per point on the jet ($\mathbf{T}(s)$ and $\mathbf{N}(s)$ must be perpendicular and $|\mathbf{T}(s)| = 1$).

Let us estimate the relative size of the terms in (6). For any spherically symmetric lens the Einstein ring radius, λ_E , is the solution to

$$\lambda_E^2 = \frac{M(\lambda_E)}{\pi \Sigma_c} \quad (8)$$

where $M(\lambda_E)$ is the mass within a projected distance of λ_E . Images that are significantly magnified form near the Einstein radius for a spherical lens or, more generally, near critical curves (the curve \mathbf{x} where $\det[\mathbf{A}(\mathbf{x})] = 0$). The magnitude of the deflection angle near λ_E is $\alpha(x) \sim \lambda_E/\lambda_o$ so if an image is formed both near the Einstein radius of a host halo and near the Einstein radius of a subclump their contributions to the deflection will differ by a factor of $\sim (\sigma_{\text{clump}}/\sigma_{\text{host}})^2$. The matrices (4) involve further derivatives of the lensing potential so that at the same point the two contributions to $\mathbf{A}_{ij}(\mathbf{x})$ will be roughly equivalent while the contribution to \mathbf{M}_{ijk} from the subclump will be larger than the host's by a factor of $\sim (\sigma_{\text{host}}/\sigma_{\text{clump}})^2 \sim M_{\text{host}}/m_{\text{sub}}$. For dwarf galaxy sized substructures this is $\sim 100 - 10,000$. From equation (6) we see that to generate a curvature radius of order the jet size, λ_s , $\lambda_s M_{ijk}/(\lambda_o |u|)$ needs to be $\gtrsim 1$. Roughly speaking only objects with Einstein radii of order the source size can create a bend.

It is useful to have concrete models for the lenses. For a spherically symmetric lens with a power-law mass profile ($M(r) \propto r^n$), or at least a power-law near the location of the image, the matrices (4) can be calculated directly:

$$\alpha(\tilde{\mathbf{x}}) = \frac{\lambda_E}{\lambda_o} \frac{\tilde{\mathbf{x}}}{\tilde{x}^{2-n}} \quad (9)$$

$$A_{ij} = \delta_{ij} - \frac{1}{\tilde{x}^{2-n}} \left[\delta_{ij} - (2-n) \frac{\tilde{x}^i \tilde{x}^j}{\tilde{x}^2} \right] \quad (10)$$

$$M_{ijk} = \left(\frac{\lambda_o}{\lambda_E} \right) \frac{(2-n)}{\tilde{x}^{3-n}} \left[\frac{\delta_{ij} \tilde{x}^k + \delta_{ik} \tilde{x}^j + \delta_{jk} \tilde{x}^i}{\tilde{x}} - (4-n) \frac{\tilde{x}^i \tilde{x}^j \tilde{x}^k}{\tilde{x}^3} \right] \quad (11)$$

where $\tilde{\mathbf{x}} \equiv (\mathbf{x} - \mathbf{x}_o)\lambda_o/\lambda_E$ is the image position relative to the center of the lens. Also useful is the convergence or dimensionless surface density at the Einstein radius in these power-law model: $\kappa(\lambda_E) = n/2$. For a Singular Isothermal Sphere (SIS) lens $n = 1$ and

$$\lambda_E = 4\pi \left(\frac{\sigma}{c} \right)^2 \frac{D_l D_{ls}}{D_s} \quad , \quad \rho(r) = \frac{\sigma^2}{2\pi G r^2}. \quad (12)$$

For a point mass $n = 0$ and $\lambda_E = \sqrt{m/(\pi \Sigma_c)}$.

3.2. Results for B1152+199

To determine what kind of structure could be responsible for the bend in image B of B1152+199 we fit a simple model to the data consisting of a galactic sized host lens and a single substructure near image B. The host does not strongly affect the bending of the jet as long as it is smooth on milli-arcsecond scales so a complex model is not necessary here. We use a SIS with a background shear - $\alpha^1(\mathbf{x}) =$

Substructure	Lens Model							
	σ_{host} (km s ⁻¹)	γ	m/M_E	σ (km s ⁻¹)	x^1 (mas)	x^2 (mas)	κ	μ_{core}
Point mass	313	0.20	1.0×10^{-4}	-	10.0	-9.93	0.54	-5.17
SIS	240	0.04	-	11.0	1.37	-0.97	1.09	-2.00

Table 1: The positions x^1 and x^2 are the center of the substructure with respect to the core in image B. The surface density κ and the magnification μ_{core} is at the core in image B.

$\gamma [x^1 \cos(2\theta_\gamma) + x^2 \sin(2\theta_\gamma)]$, $\alpha^2(\mathbf{x}) = \gamma [x^1 \sin(2\theta_\gamma) - x^2 \cos(2\theta_\gamma)]$. The shear breaks the azimuthal symmetry of the host lens which is necessary for it to fit the observed lens position.

The substructure is modeled as a single SIS or point mass at the redshift of the host lens. This model contains eight free parameters all together. Rusin et al. (2002) fit to each VLBA image a point source for the core and a Gaussian for the jet. The position of the cores and the centers of the Gaussian are used as model constraints. The tangent vectors and curvature are then set as if the jet were a segment of a circle that passes through these two points. The orientation of the Gaussian is reported, but using this as a tangent angle gives a jet that is qualitatively less bent than image B. This appears to be because the jet is more hyperbolic in shape than circular. However, a circular arc with a tangent angle of 60° at the center of the Gaussian reproduces the important features of the image well. The arc between the core and Gaussian center is then 28.6° and the radius of curvature is 11.6 mas. With the position of the lens galaxy the number of constraints is ten for eight model parameters. This method does not use the observed magnification ratio of the cores as a constraint so that any possible contamination from microlensing by stars is avoided.

Table 1 shows some of the parameters and properties of the models. For the point mass subclump the mass is quoted in terms of the mass within the Einstein radius which in this case is $M_E = (\sigma/c)^4 G^{-1} \Sigma_c(z_s, z_l)^{-1} = 1.6 \times 10^{11} h_{65}^{-1} (\sigma/246 \text{ km s}^{-1})^4 M_\odot$. The host velocity dispersions are not unusual for a large galaxy. The estimated circular velocity is $V_{\text{circ}} = 2^{1/2} \sigma$. The critical density for this lens is $\Sigma_c = 2.65 \times 10^9 h_{65} M_\odot \text{ kpc}^{-2}$. The negative magnifications at the core of image B indicate that it is inverted in one dimension with respect to image A.

In these models the jet source positions and the core source positions agree to less than a milli-arcsecond. The center of the lens galaxy agrees with the HST position (which is rather indistinct) to within $0.1''$. The tangent angles all agree to better than 10^{-3} . To do this the the substructure must be small, but not so small that its influence is not felt over the full extent of the image. These are very good fits, but the models are not entirely unique. To test the success of the model an arc in the position of the B image is mapped to the source and then to image A. The model is further adjusted so that the qualitative features of image A are reproduced. The results of this are displayed in Figure 1. Note that the models are very simple so it is surprising that they can more or less reproduce the straitness of image A along its full length.

A SIS subclump generally needs to be more massive than a point mass to have similar lensing effects. This is because the mass that is outside the Einstein radius is not as useful from a lensing standpoint. The point mass lens can be viewed as an approximation to any clump whose radius is smaller than its Einstein radius. This is the most efficient way of distributing the mass to maximize its lensing effects.

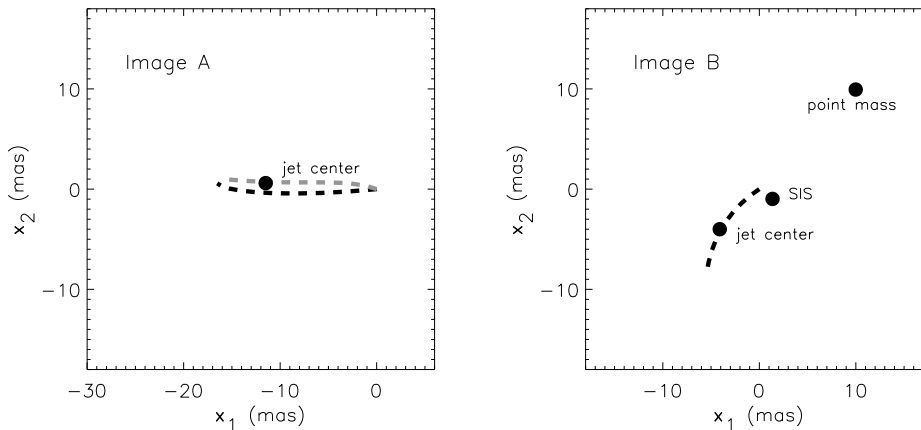


Fig. 1.— These are diagrams showing the reconstruction of Image A from an arc representing Image B using the two lens models discussed in the text. The positions of the point mass substructure and the SIS substructure are marked (only one is present in each model). The radio core is at the origin in all cases. The lighter curve in the left panel is the A image for the SIS substructure model and the darker one is for the point mass model.

4. Implications for Dark Matter and Cosmology

The structures responsible for the bend in image B of B1152+199 and the possible kink in image A of Q0957+561 are not terribly unusual in their mass or size. There are dwarf galaxies and globular clusters orbiting our galaxy that would fit the description. Its importance lies in the likelihood of such a structure being close enough to the image to cause observable bending.

4.1. Estimated substructure densities

To estimate the probability of a jet like the one in B1152+199 having an observable bend, we will consider the bending effect of a single clump acting by itself. The host lens probably enhances the effect of the clump to a small degree. This will not change the results of this section by a large amount and so this extra complication will be neglected.

If we consider a straight line in the source plane that passes by a spherically symmetric lens centered at \mathbf{x}_0 with an impact parameter of b the lensing equation (1) can be reduced to

$$b = [r \pm \alpha_r(r)] \cos(\theta) \quad , \quad r > 0 \quad (13)$$

where $r \equiv |\mathbf{x} - \mathbf{x}_0|$, θ is the corresponding axial coordinate and $\alpha_r(r)$ is the radial deflection which is < 0 . The positive sign is used for $-\pi/2 < \theta < \pi/2$ – the primary image – and the positive sign otherwise – the secondary image. We are concerned here only with the primary image; secondary images appear to form rarely in compound lensing with the mass scales considered here (Metcalf & Madau 2001) and they will generally be demagnified.

The curvature of the image can be calculated by taking derivatives of the curve (13). At the point $\theta = 0$

the curvature is $\mathbf{n}(\theta = 0) = \frac{1}{r^2} \left(\frac{d^2 r}{d\theta^2} - r \right) \hat{\mathbf{x}}$. For our two models for the subclump this is

$$\mathbf{n}(\theta = 0) = \frac{-1}{\theta_E} \begin{cases} \frac{1}{(x_b + \sqrt{x_b^2 + 4})^2} \left(\frac{3x_b^2 + 8}{\sqrt{x_b^2 + 4}} \right) \hat{\mathbf{x}} & \text{(point mass)} \\ \frac{1}{(x_b + 1)^2} \hat{\mathbf{x}} & \text{(SIS)} \end{cases} \quad (14)$$

where $x_b \equiv b/\theta_E$. For the point mass $\theta_E = \sqrt{m/(\pi D_l^2 \Sigma_c)}$ and for the SIS $\theta_E = \lambda_E(\sigma)/D_l$.

A clump will not make an observable bend in a jet of length θ_{jet} if the Einstein ring radius is either too big or too small. From (14) we see that the maximum curvature a clump can produce is $\theta_E(z)^{-1}$. When $\theta_E(z)$ is larger than the length of the jet the deviation from a straight line is at most $\sim \theta_{\text{jet}}^2/2\theta_E$. This must be larger than the smallest measurable scale, θ_{res} , which is set by either the resolution of the observations or the width of the jet. Applying this criterion to the curvature as a function of b , (14), gives an upper limit on the impact parameter. A small clump will influence a region of the jet of size $\sim \theta_E$. If the smallest scale θ_{res} is of order the circumference of the Einstein ring then its bending effects will be on too small a scale to be observed. These constraints are summarized as

$$\frac{\theta_{\text{res}}}{2\pi} \lesssim \theta_E \lesssim \frac{\theta_{\text{jet}}^2}{2\theta_{\text{res}}} \quad , \quad |\mathbf{n}(x_b)| \gtrsim \frac{2\pi\theta_{\text{res}}}{\theta_{\text{jet}}^2} \quad (15)$$

The first of these inequalities can be used to find the range of velocity dispersions or masses that could be responsible an observable bending of the jet in B1152+199:

$$6 \text{ km s}^{-1} \lesssim \sigma \lesssim 50 \text{ km s}^{-1} \quad (16)$$

$$7.1 \times 10^4 h_{65}^{-1} M_\odot \lesssim m \lesssim 4.4 \times 10^8 h_{65}^{-1} M_\odot \quad (17)$$

where the values $\theta_{\text{jet}} = 15$ milli-arcsec and $\theta_{\text{res}} = 3$ milli-arcsec have been used. This range is consistent with the σ derived in § 3.2. The true ranges are probably a bit larger because of the influence of the host lens which will increase the sensitive to smaller mass objects. The second of the inequalities (15) puts an upper limit on the impact parameter b as a function of σ or m through (14). By plugging in the smallest allowed clump we can find the largest possible impact parameter – $b \lesssim 3.7$ milli-arcsec or $23h_{65}^{-1}$ pc. The clump needs to be quite well aligned with the image.

The probability of a subclump bending the jet will be taken to be $p \propto \theta_{\text{jet}} db$ within the allowed range of b . The probability or expected number of important clumps per jet is

$$p \simeq 2\theta_{\text{jet}} \int_0^{z_s} \frac{dz}{(1+z)} \frac{D(z)^2}{H_0 E(z)} \int_{m_{\text{min}}(z)}^{m_{\text{max}}(z)} dm b_{\text{max}}(m, z) \frac{d\mathcal{N}}{dm}(m, z) \quad (18)$$

where \mathcal{N} is the 3-dimensional number density of clumps and $E(z) = [\Omega_m(1+z)^3 + \Omega_R(1+z)^2 + \Omega_\Lambda]^{1/2}$, $\Omega_R = 1 - \Omega_m - \Omega_\Lambda$. In the case of SIS lenses m can be replaced with σ and $b_{\text{max}}(z)$ can be found explicitly resulting in

$$p \simeq \theta_{\text{jet}}^2 \sqrt{\frac{2}{\theta_{\text{res}}}} \int_0^{z_s} \frac{dz}{(1+z)} \frac{D(z)^2}{H_0 E(z)} \int_{\sigma_{\text{min}}}^{\sigma_{\text{max}}} d\sigma \theta_E(\sigma, z)^{1/2} \frac{d\mathcal{N}}{d\sigma}(\sigma, z). \quad (19)$$

For the point mass case $b_{\text{max}}(m)$ must be found numerically.

To get a simple estimate of the number density of clumps required we can take them to all lie within the host lens and give them all the same velocity dispersion. In this case (19) reduces to

$$p \simeq \left(\frac{2\theta_E(\sigma)}{\theta_{\text{res}}} \right)^{1/2} \theta_{\text{jet}}^2 D_l^2 \eta(\sigma) \quad \text{(SIS)} \quad (20)$$

where $\eta(\sigma)$ is the 2-dimensional number density of clumps. For the range of allowed σ given in (16), $\eta(\sigma)/p \simeq 24 - 210 h_{65}^2 \text{ kpc}^{-2}$. This is the number density of substructures required to make the bending commonplace. The same exercise with point masses in the range $m = 10^5 - 10^7 M_\odot$ gives a range of $\eta(\sigma)/p \simeq 32 - 33 h_{65}^2 \text{ kpc}^{-2}$ or $\Sigma = 3.2 \times 10^6 - 3.3 \times 10^8 M_\odot \text{ kpc}^{-2}$ where the higher mass density is for larger mass clumps. In units of the critical density this is $\kappa = 0.001 - 0.13$. This value is anywhere from a few percent to more than all of the surface density of the host lens. The lensing effect of the host lens may reduce these estimates by a factor of roughly $|\mu|^{-1/2}$ – an estimate of the eigenvalues of the magnification matrix – which is 0.5–0.7 for the model found in § 3.2.

Instead of fixing the mass of the substructure we can guess at a realistic mass function. One expects that the number density of small mass clumps will be proportional to the density of all matter, ρ , averaged over a larger scale than the clumps being considered – constant Lagrangian number density. CDM simulations and analytic estimates predict a power-law mass function for the low mass range important here,

$$\frac{1}{\rho} \frac{d\mathcal{N}}{dm} = \frac{1}{M_o m_o} \left(\frac{m}{m_o} \right)^\alpha \quad (21)$$

where m_o and M_o are normalization constants. Using the assumption that $\sigma = 100 \text{ km s}^{-1} (m/3.0 \times 10^{11} M_\odot)^{1/3}$ this can also be converted into a distribution of velocity dispersions. In Λ CDM simulations the dark matter clumps have $\alpha \simeq -1.91$ and $M_o = 4.8 \times 10^{12} h^{-1} M_\odot$ for $m_o = 3.0 \times 10^{11} M_\odot$ (Klypin et al. 1999). The exponent for the σ distribution is $\alpha_\sigma = -3.73$ in this case. This distribution fits the observed distribution of dwarf galaxies near $\sigma = 50 - 100 \text{ km s}^{-1}$ above which the contribution to (19) is small.

Using the full range of masses in (16) and keeping all the subclumps at the redshift of the host lens results in a probability of $p \simeq 12.6 \kappa$ where κ is the surface density of the host lens, $\kappa = 0.5 - 1.4$ for the model in § 3.2. Figure 2 shows p and the fraction of the halo mass density contained in substructure as a function of a lower mass cutoff in the mass function. The smaller mass clumps contribute most of the probability, but little of the mass density. This mass fraction is a lower limit in that if the internal structure of the subclumps is less centrally concentrated it will require more mass to reach the same probability. For SIS substructures that are not tidally truncated $p = 7.3 \times 10^{-3} \kappa$. To increase this probability by a factor of ten would require the entire mass density of the host lens to be composed of SISs in the range (16). Any tidal truncation will reduce SIS substructures’ lensing effect.

Objects that are not in the host galaxy, but happen to lie near the line of sight could also cause bending of the jet. To estimate this contribution we integrate (18) with the mass function (21) assuming that ρ along the line of sight is given by the average density of the universe. For SIS structure $p = 3.7 \times 10^{-4}$ and for point masses with the same mass function $p = 2.7$. This extra-galactic population is only an important contribution to the probability if the clumps are very compact.

The CDM model does seem capable of accounting for the bent jets, provided DM halos are relatively compact. If the radius is small compared to the Einstein radius of a point mass of the same mass ($r \lesssim \theta_E = 11(m/10^6 M_\odot)^{1/2} h_{65}^{1/2} \text{ pc}$) less than $\sim 10\%$ of the mass need be in substructure. However, any less concentrated clumps will require more total mass. The SISs require much more mass. The Navarro, Frenk & White (NFW) profile (Navarro, Frenk, & White 1997), $\rho(r) = \rho_c r_s^3 r^{-1} (r_s + r)^{-2}$, is believed to be more realistic for pure dark matter halos. If r_s is small compared to the above limit and a large fraction of the mass is within this radius then the mass fraction might get down to the levels shown in figure 2. The scale length according to the standard structure formation scenario is $r_s = 2.17 \times 10^3 c^{-1} h_{65}^{-2/3} (m_{200}/10^6 M_\odot)^{1/3} \text{ pc}$ where c is the concentration and m_{200} is the virial mass. If the concentration is 100 or larger then the core is compact enough, but in this case the mass within r_s is less than 10% of m_{200} . In addition, $c \simeq 100$ is a

bit high for a straightforward extrapolation of the simulations (Bullock et al. 2001); no simulation has been done with a resolution high enough to resolve these mass scales. To achieve the same probability for bending the jet, it seems that any realistic CDM model will require significantly more mass – at least before tidal stripping occurs – to be in small scale structure than is required in the point mass model used here.

Also, the survival of substructure in the host lens is a complicated issue. Clumps with $m \gtrsim 10^7 M_\odot$ are not likely to survive within the inner few kpc because they lose orbital energy to dynamical friction and fall into the center of the galaxy where they are destroyed by tides. This upper mass cutoff can significantly change the local fraction of mass in substructures while not affecting the lensing probability greatly.

4.2. Contribution from known structures

There are about 40 known dwarf galaxies in the Local Group (Mateo 1998; Klypin et al. 1999). Most of these are within ~ 300 kpc of either the MW or M31. About twenty eight of these have circular velocities above 10 km s^{-1} . This gives an estimated surface number density of $\sim 3.5 \times 10^{-5} \text{ kpc}^{-2}$ if they were uniformly distributed in this volume. There are about 200 globular clusters in the MW with masses of $10^4 - 10^6 M_\odot$ making their number density an order of magnitude larger. The concentration of dwarfs and globular clusters toward the center of the galaxy and observational incompleteness might increase this estimate by a factor of several, but nowhere near enough to reach the required number densities derived above.

Another way of estimating the contribution from dwarf galaxies is to use the mass function (21) converted to velocity dispersion. For the observed galaxies within $200h^{-1}$ kpc of the MW and M31 $\alpha_\sigma = -2.35 \pm 0.4$ and $m_o \simeq M(< 200)/6.32$ for $\sigma_o = 10 \text{ km s}^{-1}$ where $M(< 200)$ is the total mass within $200h^{-1}$ kpc (Klypin et al. 1999). We will use $M(< 200) = 10^{12} M_\odot$. With SIS dwarf galaxies this velocity distribution gives a probability for bending the jet of $p = 2.6 \times 10^{-5} \kappa$ if the dwarfs are in the host lens. Figure 2 shows p as a function of a lower σ cutoff which is converted into mass by $\sigma = 100 \text{ km s}^{-1} (m/3.0 \times 10^{11} M_\odot)^{1/3}$. If the same velocity distribution is used for the entire line of sight at the average mass density, $p = 1.6 \times 10^{-6}$. Dwarf galaxies are not compact enough to be considered point mass lenses, but by treating them as point masses we can get an (probably greatly inflated) upper limit on the probability. In this case $p = 1.6 \times 10^{-3} \kappa$.

Known types of substructure within the host lens are inadequate to explain B1152+199. If the structures in the lens and in intergalactic space are similar in number and central density to those observed in the local group of galaxies they fall short of the estimates derived in § 4.1 by at least a factor of 10^5 .

5. Discussion

These observations have important consequences for the Warm Dark Matter (WDM) model. The standard WDM model is engineered to reproduce the dwarf galaxy distribution under the assumption that a galaxy forms in every small halo. It was shown in § 4.2 that the number density of dwarf galaxies is extremely unlikely to have produced the observed bent radio jets. The standard WDM model is thus ruled out. A more accurate lower limit on the DM particle mass will require more observations and more simulations of small scale structure formation in these models.

Higher resolution observations of B1152+199 are possible. These would make certain that the jet in image B is indeed bent and improve the constraints on the substructure mass. Even more interesting would

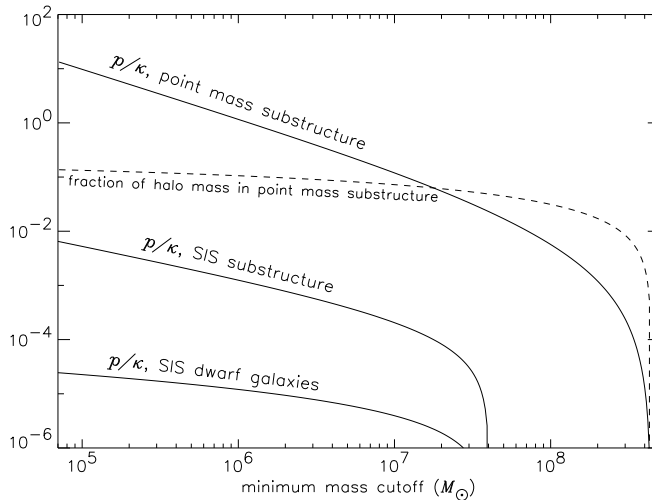


Fig. 2.— The probability of substructures causing an observable bend in a radio jet like the one in B1152+199 assuming the distribution of substructures described in the text. For the SIS substructures the velocity dispersion is converted to mass by $m = 3.0 \times 10^{11} M_{\odot} (\sigma/100 \text{ km s}^{-1})^3$. The fraction of the host halo surface density contained in point mass substructure is also plotted. The host lens surface density is $\kappa = 0.6 - 1.4$ for the model of B1152+199 discussed in § 3.2.

be high resolution images of other multiply imaged jets. In the present sample of two both appear to show some evidence of bending. A moderately larger sample would greatly increase the power of this method to probe structure on small scales.

It has been found here that a significantly larger number of small scale objects are needed. If these are compact (on the scale of their own Einstein radius) and small in mass ($\lesssim 10^7 M_{\odot}$) they need not contain a large fraction of the mass in the universe. However, such concentrated halos come about in the CDM model only through the tidal stripping of halos that originally contained ~ 10 times more mass. This means that in intergalactic space these clumps would contain a large fraction of the mass, perhaps most of it.

I would like to thank P. Madau, M. Magliocchetti and H. Zhao for useful discussions and comments. I would also like to thank D. Rusin for bringing the case of B1152+199 to my attention.

REFERENCES

- Barkana, R., Lehár, J., Falco, E. E., Grogin, N. A., Keeton, C. R., & Shapiro, I. I. 1999, *ApJ*, 520, 479
- Bode, P., Ostriker, J. P., & Turok, N. 2001, *ApJ*, 556, 93
- Bradač, M., Schneider, P., Steinmetz, M., Lombardi, M., King, L., & Porcas, R. 2002, preprint, astro-ph/0112038
- Bullock, J. S., Kolatt, T. S., Sigad, Y., Somerville, R. S., Kravtsov, A. V., Klypin, A. A., Primack, J. R., & Dekel, A. 2001, *MNRAS*, 321, 559
- Bullock, J. S., Kravtsov, A. V., & Weinberg, D. H. 2000, *ApJ*, 539, 517

- Chiba, M. 2002, *ApJ*, 565, 17
- Dalal, N. & Kochanek, C. 2002, preprint, astro-ph/0111456
- Garrett, M. A., Calder, R. J., Porcas, R. W., King, L. J., Walsh, D., & Wilkinson, P. N. 1994, *MNRAS*, 270, 457
- Kamionkowski, M. & Liddle, A. 2000, *PRL*, 84, 4525
- Keeton, C. 2002, preprint, astro-ph/0112350
- Klypin, A., Kravtsov, A. V., Valenzuela, O., & Prada, F. 1999, *ApJ*, 522, 82
- Mao, S. & Schneider, P. 1998, *MNRAS*, 295, 587
- Mateo, M. L. 1998, *ARA&A*, 36, 435
- Metcalf, R. 2001, in *Where is the Matter?*, ed. L. Tresse & M. Treyer (astro-ph/0109347)
- Metcalf, R. B. & Madau, P. 2001, *ApJ*, 563, 9
- Metcalf, R. B. & Zhao, H. 2002, *ApJ*, 567, L5
- Moore, B., Ghigna, S., Governato, F., Lake, G., Quinn, T., Stadel, J., & Tozzi, P. 1999, *ApJ*, 524, L19
- Myers, S. T., Rusin, D., Fassnacht, C. D., Blandford, R. D., Pearson, T. J., Readhead, A. C. S., Jackson, N., Browne, I. W. A., et al., 1999, *AJ*, 117, 2565
- Navarro, J. F., Frenk, C. S., & White, S. D. M. 1997, *ApJ*, 490, 493
- Rusin, D., Norbury, M., Biggs, A. D., Marlow, D. R., Jackson, N. J., Browne, I. W. A., Wilkinson, P. N., & Myers, S. T. 2002, *MNRAS*, 330, 205
- Somerville, R. S. 2002, preprint, astro-ph/0107507
- Spergel, D. N. & Steinhardt, P. J. 2000, *Physical Review Letters*, 84, 3760
- van den Bosch, F. C., Robertson, B. E., Dalcanton, J. J., & de Blok, W. J. G. 2000, *AJ*, 119, 1579
- Walsh, D., Carswell, R. F., & Weymann, R. J. 1979, *Nature*, 279, 381
- Wambsganss, J. & Paczynski, B. 1992, *ApJ*, 397, L1